JOURNAL OF COMPUTATIONAL PHYSICS 108, 246–263 (1993)

Numerical Simulation of Biofilm Processes in Closed Conduits

SANDOR SZEGO

Center for Interfacial Microbial Process Engineering, Montana State University, Bozeman, Montana 59717

PASQUALE CINNELLA

Engineering Research Center for Computational Field Simulation, Mississippi State University, Mississippi State, Mississippi 39762

AND

AL B. CUNNINGHAM

Department of Civil Engineering, Montana State University, Bozeman, Montana 59717

Received August 10, 1992; accepted February 5, 1993

The present study details the derivation and application of a finite-volume-based methodology to the simulation of biofilm processes in axisymmetric reactors. Multiple space scales, ranging from the micron to the meter, and multiple time scales, ranging from the second to the day, are resolved. Unsteady problems are considered, where diffusion and biochemical reactions are the dominant physical phenomena. Moreover, moving boundaries such as the interface between biofilm and bulk liquid are accounted for. Numerical results are presented for a few test cases, and the sensitivity of the predictions to several numerical and physical parameters is studied, including time step value, number of iterations per time step, grid size, and initial conditions.

1. INTRODUCTION

Biofilm growth is an important process in many industrial conduit systems. Corrosion of tubing in water distribution systems is frequently linked to bacterial populations at corrosion sites, indicating that biofilms can influence the surface degradation [1]. The power industry is likewise plagued by reduced efficiency of heat transfer equipment caused by excessive biofilm accumulation.

In closed conduits, flow processes governing mass transport, biofilm accumulation, and the biotransformation of organic constituents are intrinsically interrelated. Suspended cells are transported to the conduit surface (substratum) where they may adsorb. Some fraction of these adsorbed cells desorb and return into suspension, perhaps through some diffusion-like process. If environmental conditions are favorable, the adsorbed cells grow, replicate, and form a matrix composed of extracellular polymer substance (EPS) which binds the cells together. The aggregate of attached cells, EPS, and other particulate matter is termed *biofilm* [2]. Once the biofilm is established, additional cells and particulate matter may attach to and detach from the biofilm surface. The net accumulation of biofilm is therefore the result of biomass added to the surface from the processes of adsorption, growth, and attachment, less the amount of mass removed by the processes of desorption and detachment.

In order to study and model biofilm behavior, an important distinction has to be made between biofilms and *biofilm systems*. Characklis [2] defines biofilm systems as consisting of five compartments:

- *Substratum*, the solid surface where the microorganisms attach;
- *Base film*, a structured accumulation of cells;
- *Surface film*, which provides the transition between the base film and the bulk liquid compartment;
- *Bulk liquid*, which carries microorganisms and substrates in solution and exchanges mass and heat with the base film through the surface;
- *Gas*, which provides aeration or removal of gaseous reaction products and is present in external flow problems.

Components of biofilm systems are microorganisms, the organic and inorganic products of their metabolism, *substrates* (defined as the growth limiting nutrients), and other nutrients. Typical *interactions* and *processes* between these components are transport (advection, diffusion), transfer (cell attachment and detachment, interfacial diffusion), and transformation (chemical reactions). The biofilm itself consists of two of the above compartments: the base film and the surface film. A very important characteristic of a biofilm

0021-9991/93 $5.00

is that a certain, typically large, portion of its volume is liquid.

An essential parameter in the study of a given system is its *geometry*. Widely studied geometries are continuous flow stirred tank reactors (CFSTR) and plug flow reactors (PFR). CFSTRs are well-mixed tanks, where a continuous flow of reactants is present, and the well-mixed bulk is constantly removed to allow for a constant bulk volume. PFRs are idealized models of pipelines, where the reactants enter the pipe at the inlet, and products leave the pipe at the outlet. Other geometries, such as porous media, are studied as well.

A considerable amount of experimental research on the kinetics of biofilm processes has been conducted in recent years [3]. The detailed mechanisms of biofilm growth, the specific biochemical reactions that take place at the biofilm interface with the liquid phase, and the effect of different biocides are examples of active research areas. On the other hand, numerical simulations of biofilm processes have not yet reached the sophistication that is typical of other sectors of industry, with aerospace and mechanical research and development firms at the forefront. One reason for the discrepancy is that it is extremely difficult to couple the equations describing all of the biofilm processes to create a simulation model capable of predicting biofilm behavior. Individual biofilm processes are inherently nonlinear and their response to changes in bulk fluid transport phenomena has not been fully documented [2]. However, numerical simulations hold enormous promise for this difficult problem. First, numerical simulations can be used to separate the processes so that each specific phenomena can be understood by itself. Then the processes can be coupled in various ways in order to better understand the effects of various couplings. This separation of processes is difficult if not totally impossible in the laboratory. Most importantly, once biofilm phenomena can be simulated at the local level, the information can be scaled up to analyze problems in industrial conduit systems.

A few models of multispecies biofilm systems have been studied in the past. Wanner and Gujer [4] propose a model that is one-dimensional in space, whereby a multispecies biofilm is attached to a solid wall and in contact with a liquid phase through an interface. The biofilm thickness is allowed to change, due to growth, sloughing, or biocide effects, and the transport of substrate elements to the different bacteria in the biofilm is modeled. The method of lines [5] is applied to reduce the partial differential equations to ordinary differential equations that have to be solved at every time step, and a standard integration package is utilized for that purpose.

More recently, the International Association on Water Pollution Research and Control (IAWPRC) issued a report [1], in which the general governing equations for the kinetics of biofilm systems are derived. Applications to a number of biofilm reactors are discussed, including trickling filters, packed beds and groundwater systems, biological fluidizer bed reactors, and rotating biological contactors. The model is applicable to two- and three-dimensional geometries, allows for moving boundaries such as the bulk liquid interface, and includes some modeling of attachment, detachment, and sloughing at the interface. Molecular diffusion, turbulent diffusion, and advection are accounted for, and a general model for transformation processes, such as biotic and abiotic reactions, is proposed. These equations are applicable to practical cases where multiple space scales exist, because the biofilm thickness is measured in micrometers and the pipe or reactor characteristic length in meters, and in some cases kilometers. Moreover, multiple time scales are present which stem from the fact that biotic reactions can have characteristic times measured in days and fluid mechanics processes can change in seconds.

Although the above-mentioned equations [1] are very general, or probably because of that, no numerical technique for their solution is proposed or advocated. Moreover, no allowance is made for temperature effects on the biofilm behavior, and the fluid mechanics of the bulk liquid is treated in a simplified manner, whereby a velocity profile is imposed for either laminar or turbulent incompressible flows.

In the present work, the base biofilm model proposed by the IAWPRC [1] is implemented and at least partially validated. Specifically, the governing equations for a multispecies biofilm model are reformulated in integral conservation form, discretized using upwind technology [6], and solved for axisymmetric geometries. The approach proposed can be extended to three-dimensional configurations due to the geometric flexibility of finite volumes and allows for a simple and straightforward representation of moving boundaries, such as the surface film.

The subject matter of this article is the following. Section 2 contains an overview of the mathematical modeling of biofilm processes in pipelines. Section 3 describes the biofilm system governing equations, which are based on the conservation of mass principle. Section 4 explains the numerical methods applied to solve the resulting coupled, non-linear partial differential equations. Finally, Section 5 presents a few results obtained with the proposed methodology for axisymmetric geometries, and in Section 6 some conclusions are drawn.

2. BIOFILM PROCESSES IN CLOSED CONDUITS

Many industrial and natural biofilm system configurations can be accurately modeled by means of the PFR geometry. Examples include natural streams, heat exchangers, oil pipes, water distribution and waste water systems, and many more. A common characteristic of the

above systems is that there exists a significant advective motion of the liquid medium (bulk compartment) that carries all reactants and products to downstream locations. In fact, this motion and the existence of radial concentration gradients in the bulk compartment are the major differences between PFRs and CFSTRs.

The "base" biofilm model that is employed in the present work [1] takes advantage of some simplifying assumptions for the treatment of the different compartments that comprise the biofilm system. In particular, the gaseous compartment is not considered in this study, which is limited to closed conduits, and no attempt is made to model substratum corrosion. Consequently, attention will be focused on three compartments: base film, surface film, and bulk liquid.

In the following, a more thorough definition of the organic and inorganic components present in a biofilm system is provided, and the three classes of interaction processes between these components (transport, transformation, and transfer) are detailed.

2.1. *Biofilm and Bulk Liquid Components*

The biofilm systems that are analyzed in the present study typically contain the following components: substrates and other nutrients, microorganisms, metabolism products, and biocides. These components can be divided into two broad classes:

- Soluble components (substrates, nutrients, biocides, inorganic products of metabolism); and
- Particulate components (microorganisms and organic polymers).

In the following passages, the first class will be referred to as substrate, although it should be clear from the above discussion that the terminology is somewhat inaccurate. Several simplifying assumptions are employed in the modeling of the "base" biofilm [1]. In particular, one liquid phase and several (N_{part}) solid phases will comprise the biofilm. Each solid phase will contain only one particulate component and will not carry any other components. Conversely, the liquid phase will carry only soluble components.

The number and the kind of unknowns in the two compartments is different. Specifically, the bulk liquid contains $N_{\text{sub}} + N_{\text{part}}$ unknowns, related to N_{sub} substrates and N_{part} particulates, respectively. The biofilm is modeled by means of $N_{\text{sub}} + N_{\text{part}} - 1$ *independent* unknowns. Considering the bulk liquid to be composed of only one (liquid) phase, the unknown quantities are the concentrations C_i, expressed as mass per unit volume of liquid, where i is an index that spans the range one to $N_{\text{sub}} + N_{\text{part}}$. In the biofilm, using the additional assumptions that volume fraction of the liquid phase ε_l and density of the solid phases ρ_j are constant, the N_{sub} substrate unknowns are still the concentrations C_i, but the $N_{\text{part}} - 1$ independent unknowns that represent the solid phases are given by the volume fractions ε_j, equal to the ratio of the volume of the jth phase to the total volume. The (trivial) relationship

$$\sum_{j=1}^{N_{\text{part}}} \varepsilon_j = 1 - \varepsilon_l \tag{2.1}$$

ensures that only $N_{\text{part}} - 1$ solid phase volume fractions are independent.

It may be useful to point out that there are other ways the concentration, or the mass, of particulates in the film can be defined, for example, biofilm particulate mass per unit substratum area (units, ML^{-2}) and biofilm particulate mass per unit reactor volume (units, ML^{-3}). Most laboratory measurement methods determine the mass of the particulates in the film using one of the above units. However, very simple conversions are possible between these units.

2.2. *Transport: Advection and Diffusion*

Transport due to advection and diffusion plays a fundamental role in the modeling of a biofilm process. In a pipeline system, advection moves components in the flow direction. Moreover, the growth of the biofilm creates an advective motion that affects the components in the film. In extreme cases, the increased biofilm thickness can reduce the pipe section, influencing the advective phenomena in the bulk liquid. The flow regime can be either laminar or turbulent, with consequent differences in both velocity profiles and transport properties.

Diffusion occurs both in the radial and axial directions. The axial diffusion is typically orders of magnitude smaller than the advection in the same direction; thus it can be omitted. Diffusion in the radial direction is a very important phenomenon. It transfers soluble and particulate components between the bulk liquid and the film. The rate of diffusion is determined by the flow regime. In laminar flow, the diffusion coefficient of a given component in the pipe is equal to the molecular diffusion of the component, while in turbulent flow conditions the diffusion coefficient varies from the eddy diffusion to the molecular one as particles move from the center of the pipe towards the wall of the pipe. Notter and Sleicher [7] give an empirical formula for determining the eddy diffusivity.

2.3. *Transformation: Chemical Reactions*

The biofilm components interact with each other via biochemical reactions. These reactions can be described by their stoichiometric and rate coefficients. Many biochemical reactions can occur at the same time in a given system, for

example, "growth" reactions for each microorganism and oxidization or reduction of inorganic chemicals. Many components can and do participate in every reaction.

Assuming that N_{rxn} reactions take place and considering only irreversible reactions (although similar considerations would apply to reversible reactions), a generic reaction i can be written as

$$\alpha_{i,1} C_1 + \cdots + \alpha_{i,k} C_k \rightarrow \alpha_{i,k+1} C_{k+1} + \cdots + \alpha_{i,L} C_L, \quad (2.2)$$

where $L = N_{\text{sub}} + N_{\text{part}}$ is the total number of components present, and $\alpha_{i,k}$ is a stoichiometric coefficient associated with the kth component in the ith reaction. Components on the left-hand side of the arrow are consumed, and components on the right-hand side are produced. In many cases, it is more convenient to rewrite Eq. (2.2) in terms of stoichiometric coefficients that are positive when the corresponding component is produced, and negative when the component is consumed. Then the previous expression becomes

$$\nu_{i,1} C_1 + \cdots + \nu_{i,k} C_k + \cdots + \nu_{i,L} C_L = 0, \quad (2.3)$$

where $\nu_{i,k} = -\alpha_{i,k}$ for the components on the left-hand side of Eq. (2.2), and $\nu_{i,k} = \alpha_{i,k}$ otherwise.

The net rate of production for a component i can be expressed as

$$W_i = \sum_{j=1}^{N_{rxn}} \nu_{j,i} P_j, \quad i = 1, 2, \ldots, N_{\text{sub}} + N_{\text{part}}, \quad (2.4)$$

where P_j is the reaction rate for the jth reaction. A specific reaction rate can be broken into contributions from the participating components,

$$P_j = \prod_{k=1}^{N_{\text{part}} + N_{\text{sub}}} T_{j,k}(C_k), \quad j = 1, 2, \ldots, N_{rxn}, \quad (2.5)$$

where $T_{j,k}$ is the reaction kinetic expression for the jth reaction involving the kth component C_k. Typical reaction kinetic expressions are:

- Zero order,

$$T_{j,k} = K_{j,k}; \quad (2.6)$$

- First order,

$$T_{j,k} = K_{j,k} C_k; \quad (2.7)$$

- Monod,

$$T_{j,k} = \frac{C_k}{K_{j,k} + C_k}; \quad (2.8)$$

- Inhibition,

$$T_{j,k} = \frac{K_{j,k}}{K_{j,k} + C_k}. \quad (2.9)$$

If a given component k does not participate in the jth reaction, then its reaction kinetic expression is a special case of the zero-order expression with $K_{j,k} = 1$. A typical reaction rate equation for a single particulate, single substrate reaction is (first order for the particulate, Monod for the substrate)

$$P_j = \mu_{\max} C_{\text{part}} \frac{C_{\text{sub}}}{K_{j,\text{sub}} + C_{\text{sub}}}, \quad (2.10)$$

where $\mu_{\max}$ is the maximum growth rate of the cell (the same for all reactions j) and $K_{j,\text{sub}}$ is called the *half saturation* coefficient of the substrate in that reaction.

2.4. *Transfer: Detachment and Attachment*

Biofilm accumulation on solid surfaces is the result of many physical and chemical processes. The most important are

- *Adsorption*, where the cells attach to the substratum surface. It can be reversible or irreversible;
- *Desorption*, where the absorbed cells can leave the substratum and reenter the bulk compartment;
- *Attachment*, where the cells in the bulk compartment attach themselves to an already existent biofilm;
- *Detachment*, where a single cell or a group of cells leave the biofilm.

In the present model an initial layer of biofilm is assumed present, thus adsorption and desorption are not included. Attachment and adsorption are very similar processes, with the exception that, in attachment, cells are captured by the film, while, in adsorption, the capturing medium is the substratum. Detachment can take at least two forms, *erosion* and *sloughing*. Erosion refers to a continuous loss of small amount of biofilm, while sloughing means rapid, massive loss of biomass.

To model the above described phenomena a net detachment expression is utilized:

$$\textit{net detachment} = \textit{detachment} - \textit{attachment}. \quad (2.11)$$

This expression describes the net flux of particulate mass leaving the biofilm surface. It is also important to note that this process is assumed to be present at the interface only, which is a modeling approximation of insufficiently known

accuracy. Current research efforts try to determine the important parameters that influence the magnitude of detachment and/or attachment [3]. In the present model the interface flux of particulate mass R_{det} is a quadratic function of the biofilm thickness L_F,

$$R_{det} = a_2 L_F^2 + a_1 L_F + a_0, \tag{2.12}$$

where the coefficients a_i are determined by curve fits of experimental values.

3. GOVERNING EQUATIONS

The equations that govern the time and space behavior of the combined bulk liquid/biofilm system can be written in integral form, valid for an arbitrary control volume Ω bounded by a control surface $\mathscr{S}$. This formulation is consistent with the numerical algorithm to be discussed in the next section and allows for a straightforward treatment of the liquid/biofilm interface (surface film), as will be detailed in the following. The control surface $\mathscr{S}$ is allowed to move and deform with a pointwise velocity $\mathbf{u}_\Omega$.

At the present time, the velocity in the liquid phase is imposed as either a parabolic (laminar) or a power-law (turbulent) profile. Consequently, only continuity equations for the different species present in the two compartments are utilized, and the solution of the momentum equations is avoided. Moreover, temperature changes and their effects upon the physical and chemical characteristics of the system are not considered. However, the present model is capable of resolving unsteady phenomena, such as species growth/decay, in the presence of moving boundaries, such as the interface.

The governing equations are written for both biofilm and bulk liquid compartments. In addition, the interface boundary conditions, which include the modeling of attachment and detachment, play a key role in the formulation. Utilizing the definitions given in Section 2, the governing equations for both compartments may be written in the general form

$$\frac{\partial}{\partial t}\iiint_\Omega \mathbf{Q}\, d\Omega + \oint_{\mathscr{S}} (\mathbf{S} - \mathbf{S}_v)\cdot \mathbf{n}\, d\mathscr{S} = \iiint_\Omega \mathbf{W}\, d\Omega, \tag{3.1}$$

where $\mathbf{Q}$ is the vector of unknowns, $\mathbf{S}$ and $\mathbf{S}_v$ represent inviscid (convective) and viscous (diffusive) fluxes, respectively, and $\mathbf{W}$ is the vector of source terms. All of the above vectors have a length of $N_{sub} + N_{part}$ in the bulk liquid compartment, and $N_{sub} + N_{part} - 1$ in the biofilm. The first contribution to the left-hand side represents unsteady phenomena, the second term corresponds to flux in and out of the control volume Ω, and the sum of the previous two terms is balanced by production and/or disappearance of species mass within the control volume. The unit vector $\mathbf{n}$ is the local normal to the infinitesimal surface element $d\mathscr{S}$.

In the bulk liquid compartment, the vectors $\mathbf{Q}$ and $\mathbf{W}$ read

$$\mathbf{Q} = \begin{pmatrix} \varepsilon_l C_1 \\ \varepsilon_l C_2 \\ \vdots \\ \varepsilon_l C_{N_{sub}} \\ \varepsilon_l C_{N_{sub}+1} \\ \varepsilon_l C_{N_{sub}+2} \\ \vdots \\ \varepsilon_l C_{N_{sub}+N_{part}} \end{pmatrix}, \quad \mathbf{W} = \begin{pmatrix} W_1 \\ W_2 \\ \vdots \\ W_{N_{sub}} \\ W_{N_{sub}+1} \\ W_{N_{sub}+2} \\ \vdots \\ W_{N_{sub}+N_{part}} \end{pmatrix}, \tag{3.2}$$

where the liquid phase volume fraction ε_l is explicitly present for consistency with the biofilm equations, to be discussed shortly, but is identically equal to one in the present model. The source terms have been defined in Section 2, e.g., Eq. (2.4). The inviscid and viscous flux vectors read

$$\mathbf{S} = \begin{pmatrix} \varepsilon_l C_1(\mathbf{u}-\mathbf{u}_\Omega) \\ \varepsilon_l C_2(\mathbf{u}-\mathbf{u}_\Omega) \\ \vdots \\ \varepsilon_l C_{N_{sub}}(\mathbf{u}-\mathbf{u}_\Omega) \\ \varepsilon_l C_{N_{sub}+1}(\mathbf{u}-\mathbf{u}_\Omega) \\ \varepsilon_l C_{N_{sub}+2}(\mathbf{u}-\mathbf{u}_\Omega) \\ \vdots \\ \varepsilon_l C_{N_{sub}+N_{part}}(\mathbf{u}-\mathbf{u}_\Omega) \end{pmatrix}, \tag{3.3}$$

$$\mathbf{S}_v = \begin{pmatrix} D_1 \nabla C_1 \\ D_2 \nabla C_2 \\ \vdots \\ D_{N_{sub}} \nabla C_{N_{sub}} \\ D_{N_{sub}+1} \nabla C_{N_{sub}+1} \\ D_{N_{sub}+2} \nabla C_{N_{sub}+2} \\ \vdots \\ D_{N_{sub}+N_{part}} \nabla C_{N_{sub}+N_{part}} \end{pmatrix},$$

where $\mathbf{u}$ is the (imposed) velocity profile in the liquid phase, and D_i is the diffusion coefficient for species i, which will account for both laminar and turbulent diffusion. A relatively simple model for diffusion, based upon Fick's law, has been utilized.

The vector entries for the biofilm compartment are

slightly different from the ones already examined. The vectors **Q** and **W** read

$$\mathbf{Q}=\begin{pmatrix}\varepsilon_l C_1\\ \varepsilon_l C_2\\ \vdots\\ \varepsilon_l C_{N_{\text{sub}}}\\ \varepsilon_1\rho_1\\ \varepsilon_2\rho_2\\ \vdots\\ \varepsilon_{N_{\text{part}}-1}\rho_{N_{\text{part}}-1}\end{pmatrix},\quad \mathbf{W}=\begin{pmatrix}W_1\\ W_2\\ \vdots\\ W_{N_{\text{sub}}}\\ W_{N_{\text{sub}}+1}\\ W_{N_{\text{sub}}+2}\\ \vdots\\ W_{N_{\text{sub}}+N_{\text{part}}-1}\end{pmatrix}, \tag{3.4}$$

and inviscid and viscous flux vectors become

$$\mathbf{S}=\begin{pmatrix}-\varepsilon_l C_1\mathbf{u}_\Omega\\ -\varepsilon_l C_2\mathbf{u}_\Omega\\ \vdots\\ -\varepsilon_l C_{N_{\text{sub}}}\mathbf{u}_\Omega\\ \varepsilon_1\rho_1(\mathbf{u}_s-\mathbf{u}_\Omega)\\ \varepsilon_2\rho_2(\mathbf{u}_s-\mathbf{u}_\Omega)\\ \vdots\\ \varepsilon_{N_{\text{part}}-1}\rho_{N_{\text{part}}-1}(\mathbf{u}_s-\mathbf{u}_\Omega)\end{pmatrix},\quad \mathbf{S}_v=\begin{pmatrix}D_1\nabla C_1\\ D_2\nabla C_2\\ \vdots\\ D_{N_{\text{sub}}}\nabla C_{N_{\text{sub}}}\\ 0\\ 0\\ \vdots\\ 0\end{pmatrix}, \tag{3.5}$$

where some additional simplifying assumptions are utilized: the velocity of the liquid phase in the biofilm is taken to be zero, the advective velocity of the solid phases $\mathbf{u}_s$ is supposed to be equal for all of the solid phases [1, 4], and the solid phase diffusion is neglected. Moreover, the liquid phase diffusion is laminar only.

In the above, the convective velocity in the bulk liquid $\mathbf{u}$ is known (imposed), but the solid phase velocity in the biofilm $\mathbf{u}_s$ has not been determined. An equation for $\mathbf{u}_s$ may be derived by writing the N_{part} governing equations for the solid phases using a *fixed* control volume. It may be useful to reiterate that $N_{\text{part}}-1$ of these equations are independent and have been presented in Eqs. (3.1), (3.4), and (3.5). Dividing each equation by ρ_j, summing, and utilizing Eq. (2.1) yields the integral equation

$$\oint_{\mathscr{S}}\mathbf{u}_s\cdot\mathbf{n}\,d\mathscr{S}=\frac{1}{1-\varepsilon_l}\iiint_{\Omega}\left(\sum_{j=1}^{N_{\text{part}}}\frac{W_{N_{\text{sub}}+j}}{\rho_j}\right)d\Omega, \tag{3.6}$$

which may be written in differential form, using Gauss' theorem,

$$\nabla\cdot\mathbf{u}_s=\frac{1}{1-\varepsilon_l}\sum_{j=1}^{N_{\text{part}}}\frac{W_{N_{\text{sub}}+j}}{\rho_j}. \tag{3.7}$$

The previous result is not enough in itself to determine magnitude and direction of the vector $\mathbf{u}_s$. However, the direction of biofilm growth is known (or assumed) to be essentially one-dimensional in the direction perpendicular to the solid wall, and the previous result may be simplified to

$$\frac{du_s}{dz}=\frac{1}{1-\varepsilon_l}\sum_{j=1}^{N_{\text{part}}}\frac{W_{N_{\text{sub}}+j}}{\rho_j}, \tag{3.8}$$

where z is a space coordinate in the direction perpendicular to the solid wall, and u_s is the magnitude of the velocity vector $\mathbf{u}_s$. This ordinary differential equation may be solved for u_s in the whole biofilm, given the biofilm properties and the initial condition $u_s=0$ at the solid wall.

Equations (3.1) and (3.8) are sufficient to describe the behavior of this multispecies biofilm/bulk liquid system, when complemented with appropriate boundary conditions. Specifically, at a solid wall the fluxes will be zero, at the centerline of an axisymmetric problem a symmetry condition of the kind

$$\left.\frac{\partial\mathbf{Q}}{\partial n}\right|_{\text{axis}}=0 \tag{3.9}$$

will be valid, inlet flow conditions will be specified, and outlet flow conditions will be extrapolated from the interior solution.

The interface treatment is the remaining problem to be considered in order to achieve a well-posed description of the biofilm/bulk liquid system. In general, the interface will be moving in time, due to the growth/decay of the bacterial species. A relatively straightforward description of the interface behavior can be arrived at if control volume ideas are employed. Specifically, the interface may be considered to coincide with a control surface at all times, separating a control volume in the bulk liquid from a control volume in the biofilm. In general, both control volumes will move and deform in time in order to follow the interface movement. Then, a general boundary condition can be derived at the interface [1]. It may be interesting to point out to the reader familiar with elementary gas dynamics that the derivation of this boundary condition is virtually identical to the derivation of the Rankine–Hugoniot jump conditions, valid across a surface of discontinuity in a gas flow. This should not be surprising, due to the fact that the interface is also a surface of discontinuity for the par-

ticulates in suspension in the bulk liquid and for the solid phases in the biofilm. The final result for the interface boundary condition reads

$$[\![(\mathbf{S}-\mathbf{S}_v)\cdot\mathbf{n}_I]\!]=(\mathbf{R}_F\cdot\mathbf{n}_I), \tag{3.10}$$

where the notation $[\![(\cdot)]\!]$ indicates a *jump* of a given quantity, which is the difference between values to the right and to the left of a surface. The vector $\mathbf{R}_F$ represents *surface* source/sink terms, related to production or loss of mass at the surface (the transfer processes). Physically, this generalized boundary condition relates the jump in *relative* fluxes to surface source terms, where the subscript F stands for biofilm properties. The unit vector $\mathbf{n}_I$ is normal to the interface and is directed from the biofilm towards the bulk liquid. The entries in $\mathbf{R}_F$ are vectors oriented with the direction of growth, which is again assumed to be orthogonal to the solid wall. A positive source term represents biofilm growth.

Specializing the general interface boundary condition, Eq. (3.10), to the different species present in bulk liquid and biofilm, yields specific equations that can be used to close the mathematical problem given by Eqs. (3.1) and (3.8). The substrate species have no surface source/sink effects at the interface; consequently the boundary condition reduces to a statement of continuity of relative fluxes at the interface

$$\begin{aligned}(\mathbf{u}-\mathbf{u}_\Omega)\cdot\mathbf{n}_I(\varepsilon_I C_i)_B-[D_i(\nabla C_i)\cdot\mathbf{n}_I]_B\\ =-\mathbf{u}_\Omega\cdot\mathbf{n}_I(\varepsilon_I C_i)_F-[D_i(\nabla C_i)\cdot\mathbf{n}_I]_F,\\ i=1,2,\ldots,N_{\text{sub}},\end{aligned} \tag{3.11}$$

where the subscript B stands for bulk liquid conditions and the subscript F stands for biofilm properties. The above equation has been simplified by means of the assumption that the velocity $\mathbf{u}$ is zero at the interface. Moreover, it may be noted that the diffusion flux will be well defined only if the substrate concentrations C_i are continuous across the interface. However, in general the concentration *gradients* will not be continuous across the interface, as can be inferred from Eq. (3.11) when taking into account that ε_I changes from the bulk liquid value of one to the biofilm value of $1-\sum_j^{N_{\text{part}}}\varepsilon_j$.

The boundary conditions for the particulate species suspended in the bulk liquid will include interfacial transfer processes, namely those due to flocculation or deposition, erosion, and sloughing. It reads

$$\begin{aligned}(\mathbf{u}-\mathbf{u}_\Omega)\cdot\mathbf{n}_I(\varepsilon_I C_{N_{\text{sub}}+j})_B-[D_{N_{\text{sub}}+j}(\nabla C_{N_{\text{sub}}+j})\cdot\mathbf{n}_I]_B\\ =[(\mathbf{R}_j)_F\cdot\mathbf{n}_I],\quad j=1,2,\ldots,N_{\text{part}},\end{aligned} \tag{3.12}$$

where the transfer processes appear in the source term $(\mathbf{R}_j)_F$. The magnitude of the vector entry $(\mathbf{R}_j)_F$ has been given in Section 2 as a simple equation, Eq. (2.12), independent of the species j. The boundary conditions for $N_{\text{part}}-1$ solid phases in the biofilm read

$$-(\mathbf{u}_s-\mathbf{u}_\Omega)\cdot\mathbf{n}_I(\varepsilon_j\rho_j)_F=[(\mathbf{R}_j)_F\cdot\mathbf{n}_I],\quad j=1,2,\ldots,N_{\text{part}}-1. \tag{3.13}$$

Similar to the derivation of the equation for the convective velocity of the solid phases, Eq. (3.6), an expression for the component of the interface velocity $(\mathbf{u}_\Omega)_I$ normal to the interface may be derived by writing all N_{part} interface boundary conditions in the biofilm, dividing by ρ_j, summing, and recognizing that $\sum_j^{N_{\text{part}}}\varepsilon_j=1-\varepsilon_I$. The final result reads

$$(\mathbf{u}_\Omega)_I\cdot\mathbf{n}_I=\mathbf{u}_s\cdot\mathbf{n}_I+\frac{1}{1-\varepsilon_I}\sum_{j=1}^{N_{\text{part}}}\frac{(\mathbf{R}_j)_F\cdot\mathbf{n}_I}{\rho_j}. \tag{3.14}$$

At this point, an expression for the local biofilm thickness L_F can be obtained by recognizing that its time rate of change will be equal to the normal component of the interface velocity

$$\frac{dL_F}{dt}=(\mathbf{u}_\Omega)_I\cdot\mathbf{n}_I. \tag{3.15}$$

With the above boundary conditions, the system of equations given in Eq. (3.1) is well posed and allows the investigation of several important biofilm processes, as will be detailed in the following.

4. NUMERICAL FORMULATION

The governing equations presented in Eq. (3.1) are discretized in space and advanced in time using a finite-volume approach [5]. The physical domain is subdivided into a (large) number of control volumes, and the governing equations are solved for the unknown volume-averaged values of the vector $\mathbf{Q}$ at a given time. Although the present technique is applicable to arbitrary subdivisions, only *structured* meshes of control volumes will be utilized in this work. Moreover, only axisymmetric problems are analyzed in this study, which amounts to considering conduits of circular cross sections. In a structured environment, a general indexing scheme can be utilized to refer to the generic control volume in the domain, and two indexes (i, j) will be enough to describe two-dimensional or axisymmetric domains. The two indexes will roughly span "rows" and "columns" of volumes in the bulk liquid and biofilm compartments, where "rows" are approximately aligned with the flow direction, and "columns" go from the pipe wall to the centerline.

Writing the governing equations, Eq. (3.1), for the generic control volume (i, j) yields

$$\frac{\partial(\mathbf{Q}_{ij}\Omega_{ij})}{\partial t} + [(\mathbf{S}-\mathbf{S}_v)_{i+1/2,j}\cdot\mathbf{n}_{i+1/2,j}\mathscr{S}_{i+1/2,j} - (\mathbf{S}-\mathbf{S}_v)_{i-1/2,j}\cdot\mathbf{n}_{i-1/2,j}\mathscr{S}_{i-1/2,j} + (\mathbf{S}-\mathbf{S}_v)_{i,j+1/2}\cdot\mathbf{n}_{i,j+1/2}\mathscr{S}_{i,j+1/2} - (\mathbf{S}-\mathbf{S}_v)_{i,j-1/2}\cdot\mathbf{n}_{i,j-1/2}\mathscr{S}_{i,j-1/2}] = \mathbf{W}_{ij}\Omega_{ij}, \quad (4.1)$$

where volume-averaged values for $\mathbf{Q}$ and $\mathbf{W}$ have been introduced:

$$\mathbf{Q}_{ij} = \frac{1}{\Omega_{ij}}\iiint_{\Omega_{ij}} \mathbf{Q}\, d\Omega, \quad \mathbf{W}_{ij} = \frac{1}{\Omega_{ij}}\iiint_{\Omega_{ij}} \mathbf{W}\, d\Omega. \quad (4.2)$$

The surface integral has been broken into four contributions from the four boundary surfaces of control volume (i, j), whose unit normals have been indicated by $\mathbf{n}_{i\pm1/2,j}$ and $\mathbf{n}_{i,j\pm1/2}$ in the "row" and "column" directions, respectively. Surface-averaged values of the fluxes have been utilized,

$$(\mathbf{S}-\mathbf{S}_v)_{i\pm1/2,j} = \frac{1}{\mathscr{S}_{i\pm1/2,j}}\oint_{\mathscr{S}_{i\pm1/2,j}} (\mathbf{S}-\mathbf{S}_v)\, d\mathscr{S}, \quad (4.3)$$

with similar expressions for the j-direction. In the above and the following, the dot product between flux vectors or Jacobian matrices and unit normals indicates that the operation is performed on each flux or Jacobian entry. Typically, surface integral and source term contributions are grouped into a *steady state* residual, $\mathbf{R}$, and Eq. (4.1) reads

$$\frac{\partial(\mathbf{Q}_{ij}\Omega_{ij})}{\partial t} + \mathbf{R}_{ij} = 0, \quad (4.4)$$

where

$$\mathbf{R}_{ij} = [(\mathbf{S}-\mathbf{S}_v)_{i+1/2,j}\cdot\mathbf{n}_{i+1/2,j}\mathscr{S}_{i+1/2,j} - (\mathbf{S}-\mathbf{S}_v)_{i-1/2,j}\cdot\mathbf{n}_{i-1/2,j}\mathscr{S}_{i-1/2,j} + (\mathbf{S}-\mathbf{S}_v)_{i,j+1/2}\cdot\mathbf{n}_{i,j+1/2}\mathscr{S}_{i,j+1/2} - (\mathbf{S}-\mathbf{S}_v)_{i,j-1/2}\cdot\mathbf{n}_{i,j-1/2}\mathscr{S}_{i,j-1/2}] - \mathbf{W}_{ij}\Omega_{ij}. \quad (4.5)$$

The governing equations, Eq. (4.4), are advanced in time by means of a generalized three-level discretization [8]

$$\frac{(1+\psi)\,\Delta(\mathbf{Q}\Omega)^n_{ij} - \psi\Delta(\mathbf{Q}\Omega)^{n-1}_{ij}}{\Delta t^n} = (\theta-1)\,\mathbf{R}^n_{ij} - \theta\mathbf{R}^{n+1}_{ij}, \quad (4.6)$$

where the superscript n refers to the time level, the *forward difference* operator $\Delta(\cdot)$ is defined as

$$\Delta(\cdot)^n = (\cdot)^{n+1} - (\cdot)^n, \quad (4.7)$$

and ψ, θ are two parameters that take different numerical values for different classical time integration schemes. Specifically, $\psi = 0$ and $\theta = 0$ yield the Euler *explicit* scheme; $\psi = 0$ and $\theta = 1$ yield the Euler *implicit* scheme; $\psi = 0$ and $\theta = 1/2$ yield the *trapezoidal* scheme; $\psi = \frac{1}{2}$ and $\theta = 1$ yield the 3-*point backward* scheme. It may be useful to point out that the first two schemes are first-order accurate in time, whereas the other two are second-order accurate.

Starting from a known state at time level n, the equation shown is solved for the volume-averaged values of $\mathbf{Q}$ at the new time level $n+1$. When initial conditions are given (at time 0), the procedure can be started and carried out indefinitely. However, for nonzero values of the parameter θ, the right-hand side of the equation contains a contribution from the residual at the new time level, and this makes the equation *nonlinear* in the unknown $\mathbf{Q}^{n+1}$. Nonlinear equations are usually solved by using a linearization algorithm, coupled with an iterative procedure applied to the linear equations until convergence to the nonlinear solution is achieved. In the present paper, Newton's method is applied to linearize the equations. Writing the previous equation as a function L of the unknown $\mathbf{Q}^{n+1}$ yields

$$L(\mathbf{Q}^{n+1}) = \frac{(1+\psi)\,\Delta(\mathbf{Q}\Omega)^n_{ij} - \psi\Delta(\mathbf{Q}\Omega)^{n-1}_{ij}}{\Delta t^n} - [(\theta-1)\,\mathbf{R}^n_{ij} - \theta\mathbf{R}^{n+1}_{ij}] = 0; \quad (4.8)$$

and the linear scheme is obtained

$$L'(\mathbf{Q}^P)\,\Delta\mathbf{Q}^P = -L(\mathbf{Q}^P), \quad P = 0, 1, \ldots, \quad (4.9)$$

where the iteration index P is such that $\mathbf{Q}^{P=0} = \mathbf{Q}^n$, and at convergence $\mathbf{Q}^{P\to\infty} = \mathbf{Q}^{n+1}$. The function $L(\mathbf{Q})$ is called the *unsteady* residual, and $L'(\mathbf{Q})$ is its first derivative. Their expressions are slightly complicated by the fact that the control volumes are moving and deforming in time, following the growth/decay of the biofilm. After some algebra [8], it can be shown that the unsteady residual is given by

$$L(\mathbf{Q}^P) = \frac{\Omega^{P+1}_{ij}(\mathbf{Q}^P_{ij} - \mathbf{Q}^n_{ij})}{\Delta t^n} - \frac{\psi}{1+\psi}\frac{\Omega^{n-1}_{ij}\Delta(\mathbf{Q})^{n-1}_{ij}}{\Delta t^n} + \frac{\mathbf{Q}^n_{ij}}{1+\psi}[(\theta-1)\,\hat{\mathbf{R}}^n_{ij} - \theta\hat{\mathbf{R}}^P_{ij}] - \frac{1}{1+\psi}[(\theta-1)\,\mathbf{R}^n_{ij} - \theta\mathbf{R}^P_{ij}], \quad (4.10)$$

where the *geometric conservation law* established by

Thomas and Lombard [9] has been utilized to describe the volume changes due to movement and deformation, yielding a *geometric* residual $\hat{\mathbf{R}}$,

$$\hat{\mathbf{R}}_{ij} = -[\mathbf{u}_\Omega \cdot \mathbf{n}_{i+1/2,j}\mathscr{S}_{i+1/2,j} - \mathbf{u}_\Omega \cdot \mathbf{n}_{i-1/2,j}\mathscr{S}_{i-1/2,j} + \mathbf{u}_\Omega \cdot \mathbf{n}_{i,j+1/2}\mathscr{S}_{i,j+1/2} - \mathbf{u}_\Omega \cdot \mathbf{n}_{i,j-1/2}\mathscr{S}_{i,j-1/2}]. \quad (4.11)$$

In summary, the unsteady residual includes fluxes and chemistry source terms ($\mathbf{R}$), volume changes ($\hat{\mathbf{R}}$), and unsteady contributions due to time rates of change of the concentration vector $\mathbf{Q}$.

The first derivative of the unsteady residual, $L'(\mathbf{Q})$, can be easily calculated when the dependence of geometric residual and cell volumes upon the vector $\mathbf{Q}^P$ is neglected. In reality, volume changes are dictated by the growth/decay of the biofilm in time, which is a function of the concentration vector $\mathbf{Q}$. However, this functional dependence is extremely involved and its inclusion in the linearization process is impractical. Incidentally, it should be noted that as long as the linearization is not unstable, any approximation that does not excessively degrade the convergence rate to the non-linear solution is acceptable. The final result for $L'(\mathbf{Q})$ reads

$$L'(\mathbf{Q}^P) = \frac{\Omega_{ij}^{P+1}}{\Delta t^n}\mathbf{I}_{ij} + \frac{\theta}{1+\psi}\frac{\partial \mathbf{R}_{ij}^P}{\partial \mathbf{Q}}, \quad (4.12)$$

where

$$\frac{\partial \mathbf{R}_{ij}}{\partial \mathbf{Q}} = [(\mathbf{D}-\mathbf{D}_v)_{i+1/2,j}\cdot \mathbf{n}_{i+1/2,j}\mathscr{S}_{i+1/2,j} - (\mathbf{D}-\mathbf{D}_v)_{i-1/2,j}\cdot \mathbf{n}_{i-1/2,j}\mathscr{S}_{i-1/2,j} + (\mathbf{D}-\mathbf{D}_v)_{i,j+1/2}\cdot \mathbf{n}_{i,j+1/2}\mathscr{S}_{i,j+1/2} - (\mathbf{D}-\mathbf{D}_v)_{i,j-1/2}\cdot \mathbf{n}_{i,j-1/2}\mathscr{S}_{i,j-1/2}] - \frac{\partial \mathbf{W}_{ij}}{\partial \mathbf{Q}}\Omega_{ij}. \quad (4.13)$$

In the above, $\mathbf{I}$ is the identity matrix, and $\mathbf{D}$ and $\mathbf{D}_v$ are the inviscid and viscous flux Jacobians, $\mathbf{D} = \partial \mathbf{S}/\partial \mathbf{Q}$, and $\mathbf{D}_v = \partial \mathbf{S}_v/\partial \mathbf{Q}$, respectively. The matrices are indexed using the convention that they will multiply vectors $\Delta \mathbf{Q}$ evaluated *at the same locations*; i.e., matrix $\mathbf{D}_{i+1/2,j}$ multiplies $\Delta \mathbf{Q}_{i+1/2,j}$, etc.

In the previous equations, surface-averaged values were used for the discretization of inviscid and viscous fluxes, both in the residuals, Eqs. (4.5), (4.11), and in the left-hand side, Eq. (4.13). The remaining step in the discretization procedure is to relate these surface-averaged values to the unknown volume-averaged quantities, so that Eq. (4.9) can be solved and the solution advanced in time. A popular procedure [6] consists of approximating surface-averaged values of $\mathbf{Q}$ by means of extrapolation from the volume-averaged values. Using a generic index l for either i or j, two possible extrapolations are defined, one from the "right" (positive) and one from the "left" (negative)

$$\mathbf{Q}_{l\mp 1/2}^{\pm} = \mathbf{Q}_l \mp \frac{\phi}{4}[(1\pm\kappa)\nabla \mathbf{Q}_l + (1\mp\kappa)\Delta \mathbf{Q}_l], \quad (4.14)$$

where forward and backward difference operators $\Delta(\cdot)$ and $\nabla(\cdot)$ have been utilized

$$\Delta(\cdot)_l = (\cdot)_{l+1} - (\cdot)_l, \quad \nabla(\cdot)_l = (\cdot)_l - (\cdot)_{l-1}, \quad (4.15)$$

and different values of the two parameters ϕ and κ yield different kinds of space accuracy. Specifically, $\phi = 0$ yields a first-order *upwind* scheme, whereas $\phi = 1$ is necessary for all of the higher-order extrapolation formulas. In particular, $\kappa = 1$ corresponds to second-order central differences, $\kappa = -1$ results in a second-order upwind scheme, and $\kappa = \frac{1}{3}$ yields a third-order upwind-biased extrapolation [10]. On the left-hand side of the equations, only first-order extrapolations will be used for simplicity, whereas the fluxes in the unsteady residual will be approximated with one of the higher-order upwind formulas for increased accuracy.

The extrapolation formulas just discussed are used for the discretization of the inviscid fluxes in the steady residual, Eq. (4.5). Specifically, the fluxes are split in two portions, which convey the information propagating in the positive and negative directions, respectively. More details on the use of flux-split techniques in computational fluid dynamics can be found in the review article by Roe [11]. For the generic index l

$$\mathbf{S}_{l+1/2} = \mathbf{S}_{l+1/2}^{+} + \mathbf{S}_{l+1/2}^{-}, \quad (4.16)$$

where

$$\mathbf{S}_{l+1/2}^{\pm}\cdot \mathbf{n}_{l+1/2} = \frac{\tilde{\mathbf{u}}_{l+1/2}^{\mp} \pm |\tilde{\mathbf{u}}_{l+1/2}^{\mp}|}{2}\mathbf{Q}_{l+1/2}^{\mp}, \quad (4.17)$$

and the *contravariant* velocity $\tilde{\mathbf{u}}$ is defined as the component of the relative velocity normal to the surface $l+\frac{1}{2}$

$$\tilde{\mathbf{u}}_{l+1/2} = (\mathbf{u}-\mathbf{u}_\Omega)_{l+1/2}\cdot \mathbf{n}_{l+1/2}. \quad (4.18)$$

In the above, the velocity in the liquid phase $\mathbf{u}$ is extrapolated from the cell volumes to the cell faces using the same formulas discussed in Eq. (4.14). In the biofilm, $\mathbf{u}$ in Eq. (4.18) should be substituted with $\mathbf{u}_s$, which is known at the cell faces. The surface velocity $\mathbf{u}_\Omega$ is also known at the cell faces. Values that are known at the cell faces can be utilized by means of the trivial "extrapolation"

$$(\cdot)_{l+1/2}^{+} = (\cdot)_{l+1/2}^{-} = (\cdot)_{l+1/2}. \quad (4.19)$$

It might be noted that in the above formulas the positive flux contains the information that propagates from left towards right and utilizes the extrapolation formulas from the left (negative). The opposite is true for the negative flux.

The inviscid Jacobian matrices can be similarly split,

$$\tilde{\mathbf{D}}_{l+1/2}\,\Delta\mathbf{Q}_{l+1/2}=\tilde{\mathbf{D}}^{+}_{l+1/2}\,\Delta\mathbf{Q}^{+}_{l+1/2}+\tilde{\mathbf{D}}^{-}_{l+1/2}\,\Delta\mathbf{Q}^{-}_{l+1/2}$$
$$=\tilde{\mathbf{D}}^{+}_{l+1/2}\,\Delta\mathbf{Q}_{l}+\tilde{\mathbf{D}}^{-}_{l+1/2}\,\Delta\mathbf{Q}_{l+1}, \qquad (4.20)$$

where the first-order extrapolation formulas for $\Delta\mathbf{Q}$ have been utilized, and the *generalized* Jacobian matrix $\tilde{\mathbf{D}}=\mathbf{D}\cdot\mathbf{n}$ has been introduced. The generalized matrix has the simple (diagonal) form

$$\tilde{\mathbf{D}}^{\pm}_{l+1/2}=\frac{\tilde{\mathbf{u}}^{\mp}_{l+1/2}\pm|\tilde{\mathbf{u}}^{\mp}_{l+1/2}|}{2}\,\mathbf{I}. \qquad (4.21)$$

The viscous fluxes at a face $l+1/2$ are related to the *directional* derivative of concentration, in the direction orthogonal to the face itself. For species k they are given as

$$(\tilde{\mathbf{S}}_v)_k=(D_k)_{l+1/2}\,\mathbf{n}_{l+1/2}\cdot\nabla C_k=(D_k)_{l+1/2}\frac{dC_k}{dn_{l+1/2}}, \qquad (4.22)$$

where the generalized viscous flux vector $\tilde{\mathbf{S}}_v=\mathbf{S}_v\cdot\mathbf{n}$ has been introduced. The diffusion coefficient at a cell face $(D_k)_{l+1/2}$ is evaluated as the arithmetic average of the cell volumes that share the face under consideration. The directional derivative can be evaluated in terms of components in the i-direction and the j-direction. The final result reads

$$\frac{dC_k}{dn_{l+1/2}}=(\mathbf{n}_{l+1/2}\cdot\mathbf{n}_\xi)\,|\nabla\xi|\,\frac{\partial C_k}{\partial\xi}+(\mathbf{n}_{l+1/2}\cdot\mathbf{n}_\eta)\,|\nabla\eta|\,\frac{\partial C_k}{\partial\eta}, \qquad (4.23)$$

where ξ and η represent *generalized* curvilinear coordinates [5] in the i- and j-directions, and $\mathbf{n}_\xi$, $\mathbf{n}_\eta$ are their local unit normals, respectively. In most cases of practical interest, diffusion in the streamwise direction is negligible, and the only important contribution to the viscous fluxes is diffusion in the normal direction. This physical result translates into a simplified version of the viscous contributions [5], whereby the generic l-direction becomes the j-direction *only*, the variation in ξ (or i) is negligible, and the directional derivative reduces to

$$\frac{dC_k}{dn_{j+1/2}}=|\nabla\eta|\,\frac{\partial C_k}{\partial\eta}. \qquad (4.24)$$

In the above, the unit normal in the η-direction $\mathbf{n}_\eta$ coincides with $\mathbf{n}_{j+1/2}$. The concentration gradient $\partial C_k/\partial\eta$ is approximated by a second-order accurate difference, and the magnitude of the gradient in the η-direction $|\nabla\eta|$ is approximated by the ratio of the cell surface to the average cell volume

$$\left(\frac{\partial C_k}{\partial\eta}\right)_{j+1/2}=(C_k)_{j+1}-(C_k)_j,$$
$$|\nabla\eta|_{j+1/2}=\frac{\mathscr{S}_{j+1/2}}{0.5(\Omega_j+\Omega_{j+1})}. \qquad (4.25)$$

More details on the modeling of diffusion fluxes in conjunction with finite-volume techniques can be found in Walters *et al.* [12].

The viscous flux Jacobians are obtained by neglecting the variation of diffusion coefficients with respect to the vector $\mathbf{Q}$. After some algebra, they can be written as the sum of "positive" and "negative" contributions,

$$(\tilde{\mathbf{D}}_v)_{j+1/2}\,\Delta\mathbf{Q}_{j+1/2}$$
$$=(\tilde{\mathbf{D}}_v)^{+}_{j+1/2}\,\Delta\mathbf{Q}^{+}_{j+1/2}+(\tilde{\mathbf{D}}_v)^{-}_{j+1/2}\,\Delta\mathbf{Q}^{-}_{j+1/2}$$
$$=(\tilde{\mathbf{D}}_v)^{+}_{j+1/2}\,\Delta\mathbf{Q}_{j}+(\tilde{\mathbf{D}}_v)^{-}_{j+1/2}\,\Delta\mathbf{Q}_{j+1}, \qquad (4.26)$$

where

$$(\tilde{\mathbf{D}}_v)^{\pm}_{j\pm1/2}=\mp D_{j\pm1/2}\,|\nabla\eta|_{j\pm1/2}\left(\frac{1}{\varepsilon_l}\right)_j\mathbf{I}, \qquad (4.27)$$

and D represents the diffusion coefficient for the generic species.

The source terms that appear in the steady residual, Eq. (4.5), are modeled in Section 2. The source term Jacobian is evaluated in a straightforward manner.

Substitution of the previously discussed expressions for fluxes, source terms, and their Jacobians into the linearized equation, Eq. (4.9), results in a set of coupled linear equations for the volume-averaged unknowns $\Delta\mathbf{Q}^P$. Specifically, the equation written for the volume (i,j) contains values of $\Delta\mathbf{Q}^P$ for the volume (i,j) itself, and also for volumes $(i\pm1,j)$ and $(i,j\pm1)$. However, the contribution $(i+1,j)$ is due to the negative portion of the inviscid flux Jacobian only, as can be inferred from Eq. (4.20), and the contribution $(i-1,j)$ is due to the positive portion only. A close examination of the Jacobian matrices, Eq. (4.21), reveals that when the normal velocity $\tilde{\mathbf{u}}$ is positive, the negative Jacobian is identically zero, and vice versa for a negative $\tilde{\mathbf{u}}$. This justifies the use of a *marching algorithm* for the solution of Eq. (4.9) when the imposed velocity field in the streamwise direction is either positive or negative. Specifically, the governing equations are solved simultaneously for all of the volumes at a given i-station, iterating until the solution at the new time step $n+1$ is recovered, and then the procedure is repeated at the new station $i+1$ for a positive

velocity field, or $i-1$ for a negative field. At every station, a block-tridiagonal system of equations has to be solved; that is, the generic equation for volume (i, j) contains contributions for $\Delta \mathbf{Q}^P$ at volumes (i, j), $(i, j+1)$, and $(i, j-1)$ only. For a positive velocity field, the contribution $(i-1, j)$ is multiplied by $\Delta \mathbf{Q}^P_{i-1,j}$ which is zero because the previous i-station has been converged, and similarly the contribution $(i+1, j)$ is multiplied by a zero $\Delta \mathbf{Q}^P_{i+1,j}$ for a negative field. The solution procedure for block-tridiagonal systems of equations is carried out efficiently using recursive formulas [5].

It may be noted that the marching technique will not be applicable in the presence of a velocity field of mixed sign (partially separated and recirculating flow). In this case, a marching/global algorithm is necessary, where the flowfield is swept forward and backward until convergence is achieved. However, the cases presented in this paper will involve attached flows only.

At this point, the remaining quantities that have to be evaluated are the solid phase velocity $\mathbf{u}_s$ in the biofilm, and the cell surface deformation velocity $\mathbf{u}_\Omega$ in both bulk liquid and biofilm. The determination of the solid phase velocity $\mathbf{u}_s$ is based upon the integral formula, Eq. (3.6), which can be discretized and solved for the values of $\mathbf{u}_s$ at the cell faces. In the process, it becomes necessary to make the before-mentioned assumption that the direction of $\mathbf{u}_s$ is perpendicular to the solid wall. Consequently, the vector $\mathbf{u}_s$ can be written as $\mathbf{u}_s = u_s \mathbf{e}_{u_s}$, where u_s is its magnitude and $\mathbf{e}_{u_s}$ is the unit normal to the solid wall. Then, Eq. (3.6) can be discretized for the generic volume (i, j) and reads

$$[u_s(\mathbf{e}_{u_s}\cdot\mathbf{n})\,\mathscr{S}]_{i,j+1/2} - [u_s(\mathbf{e}_{u_s}\cdot\mathbf{n})\,\mathscr{S}]_{i,j-1/2} + [u_s(\mathbf{e}_{u_s}\cdot\mathbf{n})\,\mathscr{S}]_{i+1/2,j} - [u_s(\mathbf{e}_{u_s}\cdot\mathbf{n})\,\mathscr{S}]_{i-1/2,j} = \frac{1}{1-\varepsilon_l}\left(\sum_{k=1}^{N_{\text{part}}} \frac{W_{N_{\text{sub}}+k}}{\rho_k}\right)\Omega_{ij}. \tag{4.28}$$

The left-hand side of the previous expression can be dramatically simplified when the assumption is made that the streamwise direction is parallel to the solid wall, which translates into zero dot products between $\mathbf{e}_{u_s}$ and the unit normals $\mathbf{n}_{i\pm 1/2,j}$. The reduced equation

$$[u_s(\mathbf{e}_{u_s}\cdot\mathbf{n})\,\mathscr{S}]_{i,j+1/2} - [u_s(\mathbf{e}_{u_s}\cdot\mathbf{n})\,\mathscr{S}]_{i,j-1/2} = \frac{1}{1-\varepsilon_l}\left(\sum_{k=1}^{N_{\text{part}}} \frac{W_{N_{\text{sub}}+k}}{\rho_k}\right)\Omega_{ij} \tag{4.29}$$

can be solved for the vector magnitudes u_s by marching from the solid wall to the interface, using the boundary (initial) condition $u_s = 0$ at the wall.

Once the vector $\mathbf{u}_s$ has been determined for all cell faces in the biofilm and for the interface, the vector $\mathbf{u}_\Omega$ can be evaluated at the interface, using Eq. (3.14), once it is assumed that the interface source term $\mathbf{R}_{I^*}$ is also a vector whose direction is known (again, the direction perpendicular to the solid wall).

At this point, all of the values of physical interest have been determined at a given time step n and/or iteration step P. In order to advance the solution in time, it is now necessary to specify the grid movement as it evolves and deforms to follow the biofilm growth at different streamline locations. Specifically, the grid is allowed to move and deform in the j-direction only (the direction normal to the wall). Once the interface velocity is determined, all the remaining faces in the j-direction are allowed to move following a linear distribution of $\mathbf{u}_\Omega$ with space, from the full value at the interface to zero at both the centerline and the solid wall. This procedure determines the values of $\mathbf{u}_\Omega$ at all cell faces in the domain.

The final step that needs to be taken in order to evaluate the new volumes and areas for the new grid (the one that has moved with the specified deformation velocities $\mathbf{u}_\Omega$, now known) is to relate *centroid* values of $\mathbf{u}_\Omega$ to *vertex* values. Specifically, all of the vertices that define a given volume have to be moved in such a way as to have an overall face deformation velocity equal to the known value $\mathbf{u}_\Omega$. Once the location of the new vertices is established, the determination of the new volumes and surface areas is made possible. The vertex movement is started at the *outlet*, where vertex velocities are taken to have a component in the $\mathbf{e}_{u_s}$ direction equal to the $\mathbf{u}_\Omega$ in the last volume. Regressing in the streamwise direction, the vertex velocity component in the $\mathbf{e}_{u_s}$ direction is extrapolated from the known values at the cell face (the local $\mathbf{u}_\Omega$) and the previous vertices, assuming a linear variation in space. Exploiting the fact that the grid movement is not allowed in the i-direction, magnitude and direction of the vertex velocity can be evaluated from geometric considerations once the component in the $\mathbf{e}_{u_s}$ direction is known. The actual displacement of the vertices follows by multiplying the vertex velocity by the time step. The reason for chosing the outlet instead of the inlet as the starting point for the grid update lies in the fact that the axial variation of the thickness is a minimum at the outlet, as well be seen in the next section. The drawback of this approach is that only information at the time step n can be used to determine the shape of the grid at time $n+1$, because the marching algorithm requires knowledge of both old and new grids to update the solution from time n to time $n+1$. On the other hand, considering the biofilm horizontal at the inlet violates the physics of the problem, and that assumption would be required in order to start the grid update at the inlet and utilize current information to change the grid.

The implementation of the boundary conditions is straightforward when the finite-volume approach is employed. The centerline surface will collapse to a surface of zero area: at the wall a zero species gradient boundary

condition can be imposed, at the inlet concentrations are specified, and at the outlet the concentrations will be extrapolated from the interior values. The interface boundary conditions are also simplified considerably by the use of the finite-volume approach. The substrate equations will be essentially unaffected by the presence of an interface, because the relative fluxes are automatically continuous between bulk liquid and biofilm, in agreement with Eq. (3.11). The N_{part} equations in the bulk liquid and the $N_{\text{part}} - 1$ equations in the biofilm that deal with particulate species have a boundary condition of the kind illustrated in Eqs. (3.12) and (3.13), and their relative fluxes $(\mathbf{S} - \mathbf{S}_v) \cdot \mathbf{n}$ at the interface will be given by the surface source terms.

5. NUMERICAL RESULTS

Preliminary numerical results have been obtained using the approach described. A simple biofilm model consisting of one microorganism, *pseudomonas aeruginosa*, and one substrate, glucose, has been investigated, and a "standard" solution has been obtained for the time evolution of the system. Moreover, the solution sensitivity to the variation of a few control parameters—time step, number of iterations per time step, grid size in the radial and axial directions, initial thickness of the biofilm—has been studied.

The important parameters of the standard solution are the following:

- Pipe length $L = 2m$, diameter $\mathscr{D} = 4 \times 10^{-3}$ m, volume flow rate $\dot{Q} = 1.4 \times 10^{-6}$ m^3/s;
- Number of substrates $N_{\text{sub}} = 1$ (glu), number of particulates $N_{\text{part}} = 1$ (pse), number of reactions $N_{rxn} = 1$;
- Molecular diffusion coefficients,

$$D_{\text{glu,bulk}} = 6 \times 10^{-9} \text{ m}^2/\text{s}, \quad D_{\text{pse,bulk}} = 1.2 \times 10^{-9} \text{ m}^2/\text{s}, \quad D_{\text{film}}/D_{\text{bulk}} = 0.9; \tag{5.1}$$

- Particulate density and liquid phase volume fraction in the biofilm,

$$\rho_{\text{pse}} = 107 \text{ kg/m}^3, \quad \varepsilon_l = 0.8 \Rightarrow \varepsilon_{\text{pse}} = 0.2; \tag{5.2}$$

- Chemical reaction coefficients (Monod for the substrate, first order for the particulate), Eqs. (2.4), (2.5),

$$\nu_{1,\text{glu}} = -1.78, \quad \nu_{1,\text{pse}} = 1, \quad T_{1,\text{glu}} = \frac{Q_{\text{glu}}}{1.6 + Q_{\text{glu}}}, \quad T_{1,\text{pse}} = 10^{-4} Q_{\text{pse}} \quad \text{kg/m}^3\,\text{s}; \tag{5.3}$$

- Interface flux of particulate mass, Eq. (2.12),

$$R_{\text{det}} = 5 \times 10^4 L_F^2 \quad \text{kg m}^2/\text{s}; \tag{5.4}$$

- Initial concentrations, biofilm thickness,

$$C_{\text{glu}}(0) = 2 \times 10^{-2} \text{ kg/m}^3, \quad C_{\text{pse}}(0) = 0 \text{ kg/m}^3, \quad L_F(0) = 10 \ \mu\text{m}; \tag{5.5}$$

- Numerical parameters: Euler Implicit, second-order upwind,

$$\psi = 0, \quad \theta = 1, \quad \phi = 1, \quad \kappa = -1; \tag{5.6}$$

- Phsysical time step Δt,

$$\Delta t = 8.64 \ s = 1 \times 10^{-4} \ d; \tag{5.7}$$

- Grid size: number of grid points in the biofilm $N_{\text{film}} = 10$, number of grid points in the bulk liquid $N_{\text{rad}} = 21$, number of grid points in the axial direction $N_{\text{axial}} = 20$.

The geometry of the pipe and the flowrate result in a Reynolds number less than 2100; thus laminar flow regime and molecular diffusion is assumed in the pipe. The average velocity in the pipe is $v = 0.111$ m/s.

Results obtained for the "standard" case are shown in Figs. 1 through 4. The time evolution of the film thickness is plotted in Fig.1. Curve (a) shows the thickness at the inlet (actually, in the first column of finite volumes), curve (b) is in the middle of the pipe ($x = 1$ m), and curve (c) shows the outlet values (the last column of finite volumes). It is easy to see that a *steady state* is reached by the end of the first day. In fact, another run was continued for six days of simulated time, and the thickness of the film did not change more than 1%.

Figure 2 shows the thickness profiles at different times, namely at 0.1, 0.3, 0.5, and 1 days, along the pipe. In general, the thickness of the film decreases as the distance increases.

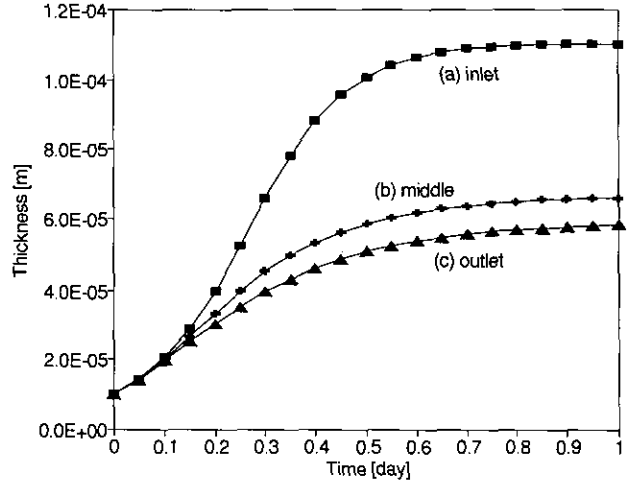

FIG. 1. Standard experiment. L_F versus time.

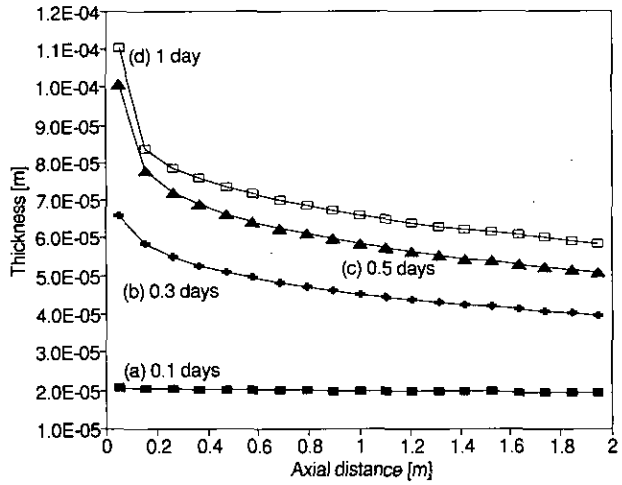

FIG. 2. Standard experiment. L_F versus axial distance.

The reason for this can easily be found by looking at Fig. 3, which shows the steady state concentration profiles of glucose and pseudomonas as a function of the axial distance from the inlet. Since the only source of glucose is at the inlet, it becomes consumed as the liquid moves in the pipe, thus less and less "food" is available for growth down the pipe. For this and the following results, the average concentrations are calculated as volume-averaged values for a given column i,

$$C_i^{\text{aver}} = \frac{\sum_j C_{ij}\Omega_{ij}}{\sum_j \Omega_{ij}}, \tag{5.8}$$

and the interface concentrations are the ones in the first volume of the bulk liquid off of the surface film.

An interesting phenomenon can also be seen by comparing average concentrations with the values at the interface. There is a large difference between the average and the interface concentrations, due to diffusional resistance. The flow regime is laminar; therefore the diffusion coefficients are very small and the diffusional distance is the entire radius of the pipe.

Figure 3 shows that both the average and interface concentrations of glucose decrease as the distance from the inlet increases. The shape of the average pseudomonas curve is also as expected, increasing monotonically from the inlet. On the other hand, the interface concentration of pseudomonas is maximum at the inlet; then it levels off and increases only slightly along the pipe length. This unexpected behavior can be explained as follows. At the interface there is a flux of pseudomonas into the bulk liquid from the film, which is a function of thickness. Molecular diffusion transfers some particulate to the next volume element in the bulk, and some (insignificant compared to the other processes) is produced by the biochemical reaction. Finally, advection transports pseudomonas in the axial direction. However, at the interface the advective velocity is very low, since the flow regime is laminar. Therefore, at the inlet a large amount of pseudomonas is produced by detachment, and only a very small fraction of it is transported to the bulk of the liquid phase. Moving downstream, the film thickness is considerably less, and so is the amount of detached pseudomonas. Consequently, the sum of the advected and detached pseudomonas is less than the previous amount. However, further downstream the change in thickness becomes less drastic, thus the sum of advection and local production will eventually increase moving downstream. This explains why there is a slight increase of interface concentration of pseudomonas. It might be useful to point out that different concentration gradients could have been observed by changing the net

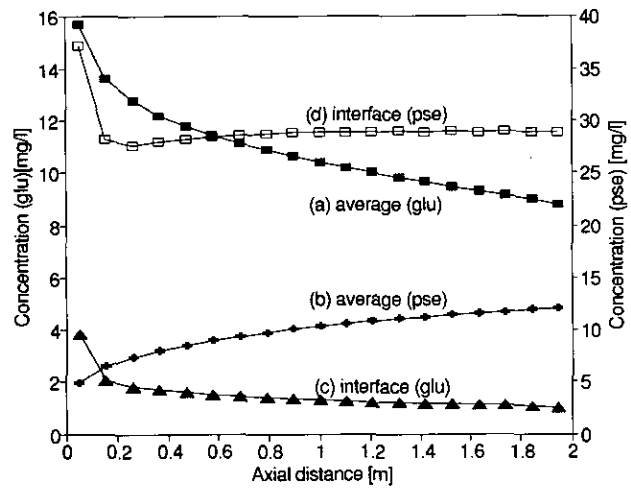

FIG. 3. Standard experiment. Average and interface concentrations versus axial distance at $t = 1d$.

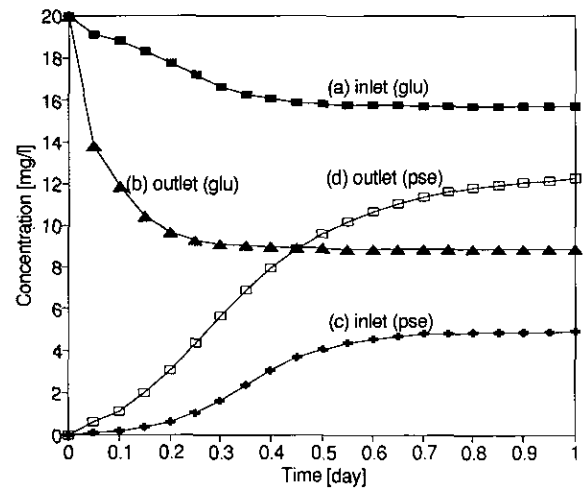

FIG. 4. Standard experiment. Average concentrations versus time.

detachment expression, Eq. (2.12), or modifying the flow regime.

The time evolution of the average glucose and pseudomonas concentrations at the inlet and the outlet is depicted in Fig. 4. As expected, the average concentration of glucose decreases with time, and the outlet concentration is always below the inlet concentration. Conversely, the average concentration of pseudomonas is constantly increasing, and the outlet is always above the inlet concentration due to advection in the downstream direction.

5.1. *Size of the Time Step*

The present version of the program uses fixed, user-supplied time steps for advancing the solution in time. Consequently, it is important to see how the accuracy of the simulation is affected by the change in time step. To this end, two experiments were attempted: the first one (run1) using a timestep of 4.32 s, or twice as small as the standard case, and the second one (run2) using 2.16 s for a timestep, or four times smaller. In order to put these timestep values into perspective, it is useful to estimate the CFL-like numbers associated with advection, diffusion, and reaction phenomena, which can be defined as

$$\mathrm{CFL}_{\mathrm{adv}} = \frac{\Delta t\, v}{\Delta x},$$

$$\mathrm{CFL}_{\mathrm{diff}} = \frac{\Delta t\, D}{(\Delta x)^2}, \tag{5.9}$$

$$\mathrm{CFL}_{\mathrm{reac}} = \frac{\Delta t}{\mu_{\max}},$$

where v is a fluid or a solid phase velocity, D is a diffusion coefficient, Δx is a spatial step, and $\mu_{\max}$ is a chemical reaction characteristic time, most often the coefficient of the first-order reaction rate expression, Eq. (2.10). Typically, explicit integration systems are stable if the CFL-like number is less than one. Implicit systems are usually unconditionally stable, if the partial differential equations are linear. However, for accurate resolutions of unsteady phenomena, the CFL number has to be kept at a moderate value. For nonlinear systems, such as the present model, the CFL number can be greater than one, but in extreme cases the algorithm might become unstable. The CFL-like numbers for the standard run are (at $t = 0$):

$$\begin{aligned} \mathrm{CFL}_{\mathrm{adv,axial}} &\approx 9.1, \\ \mathrm{CFL}_{\mathrm{adv,radial}} &\approx 0.1, \\ \mathrm{CFL}_{\mathrm{diff}} &\approx 5.1 \times 10^4, \\ \mathrm{CFL}_{\mathrm{reac}} &\approx 9.2 \times 10^4. \end{aligned} \tag{5.10}$$

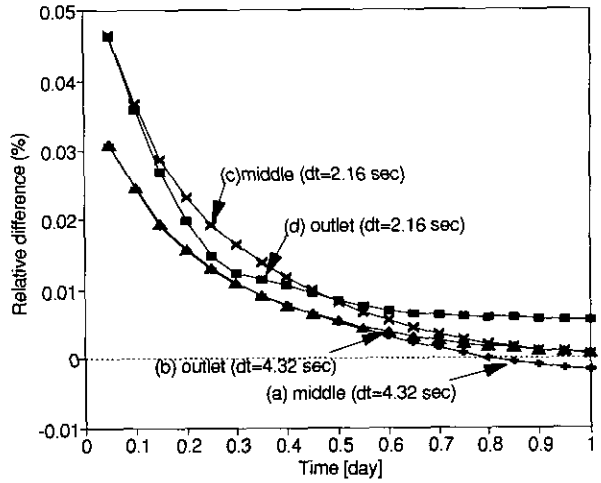

FIG. 5. Relative difference between the standard experiment and run1 and run2 (L_F).

It is clear that the advection is resolved in time, unlike the physical transient associated with diffusion and chemical reactions. Moreover, $\mathrm{CFL}_{\mathrm{diff}}$ and $\mathrm{CFL}_{\mathrm{reac}}$ are much greater than one, leading to the possibility of instabilities. As a matter of fact, when the timestep of the standard calculation was doubled, the run aborted.

A sample of the results is shown in Figs. 5 and 6. In Fig. 5, curves (a) and (b) represent the relative difference between the biofilm thickness obtained with run1 and the one obtained by means of the standard calculation, in the middle of the domain and at the outlet, respectively. Curves (c) and (d) show the relative difference between run2 and the standard. It may be noted that the difference approaches zero as the calculation approaches a steady state, consistent with the fact that only the time discretization was affected by the experiment. Moreover, the maxi-

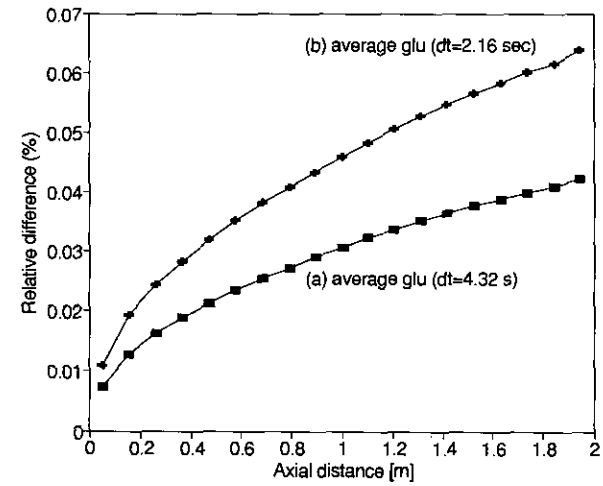

FIG. 6. Relative difference between the standard experiment and run1 and run2 ($C_{\mathrm{glu}}^{\mathrm{aver}}$ at $t = 1d$).

mum difference shown is less than 0.05%, although this is not the maximum difference between the runs. At the very first time steps one can expect even larger relative differences (these graphs show the values at every 500 time steps, thus the initial events are missing). Since the thickness of the film is very small near the initial state, even larger *relative* differences can still mean very small *absolute* differences.

The relative differences of the average concentration of glucose at $t = 1d$ are shown in Fig. 6. Curves (a) and (b) represent the relative difference between the standard calculation and run1 and run2, respectively. In this case, the relative difference increases as the distance from the inlet increases, because the marching algorithm will propagate errors and inaccuracies downstream. It is important to point out that the relative differences are very small, ranging from 0.01 to 0.06%.

5.2. *Number of Iterations per Time Step*

Another numerical parameter in the algorithm is the number of iterations performed at each time step. Ideally, the unsteady residual should be fully converged at each time step. This is particularly true when there are differences between the order of accuracy of the space discretizations utilized in the left- and right-hand sides of the equations, as is the case here. In the present calculations, 10 iterations per time step were performed, significantly more than the two to four deemed sufficient in the current literature [13]. In order to test this choice, two additional runs were made, one with five iterations per time step (run3), the other using only two iterations (run4).

The relative difference between the thickness values at the inlet and the outlet as a function of time for both cases is shown in Fig. 7. Until 0.4 days the differences for both runs are negligible. Afterwards, the relative difference in inlet thickness becomes more significant. This is probably due to the nonlinear nature of the reaction rates, which is particularly significant at the inlet and which translates into significant unsteady effects. On the other hand, the Monod kinetics becomes approximately linear for low concentrations of glucose, which is the case at the outlet after the initial transient, thus only one Newton iteration would suffice to advance the integration, as shown by curves (c) and (d) in Fig. 7.

The differences in concentrations, not represented here, support the statements made above. Again, the largest differences are near the inlet, which is the result of the more nonlinear behavior of the Monod kinetic expression. Near the outlet all concentrations are almost identical.

5.3. *Grid Convergence Study*

The accuracy of the predictions obtained was tested by performing a grid convergence study. In the first test (run5), the number of radial grid points in the bulk liquid was doubled to $N_{\text{rad}} = 41$, whereas the second test (run6) featured a more refined grid in the axial direction, with $N_{\text{axial}} = 39$. Finally, both radial and axial grid sizes were doubled, and a third test (run7) was conducted ($N_{\text{film}} = 10$, $N_{\text{radial}} = 41$, $N_{\text{axial}} = 39$). The number of grid points in the biofilm was left unchanged, because the overall thickness of the film does not exceed a few microns, which is three orders of magnitude smaller than the radial distance.

The biofilm thickness profiles at $t = 1d$ obtained with the standard run and the new runs are shown in Fig. 8. Some discrepancies can be seen in the first few volumes, approximately until $x = 0.6$ m. Figure 9 shows the relative differences between the previous runs. The solution is more sensitive to the axial refinement that the one in the radial direction, and the maximum discrepancies occur again at the inlet region. Overall, although the results are not

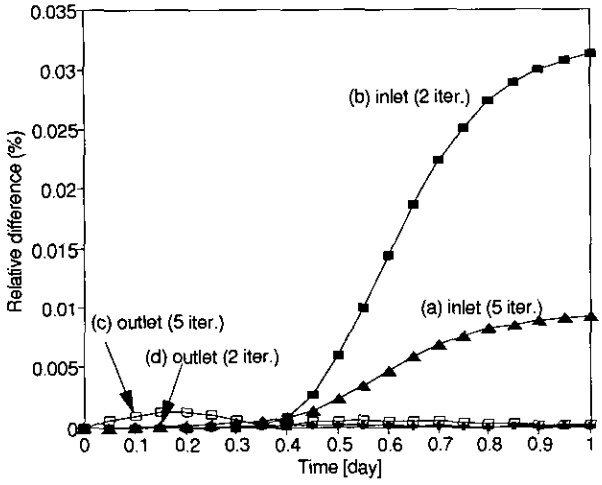

FIG. 7. Relative difference between the standard experiment and run3 and run4 (L_F).

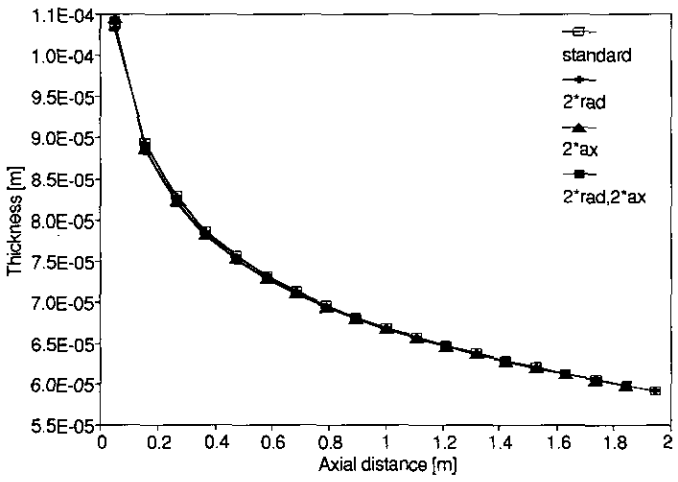

FIG. 8. Biofilm thickness L_F at $t = 1d$: standard, run5, run6, and run7.

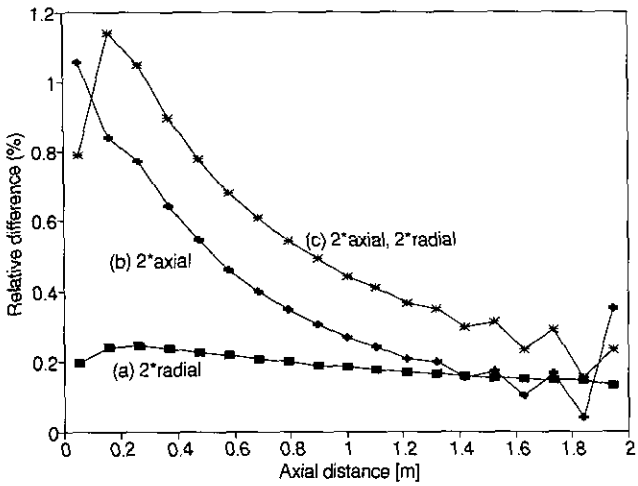

FIG. 9. Relative difference between the standard experiment and run5, run6, and run7 (L_F at $t = 1d$).

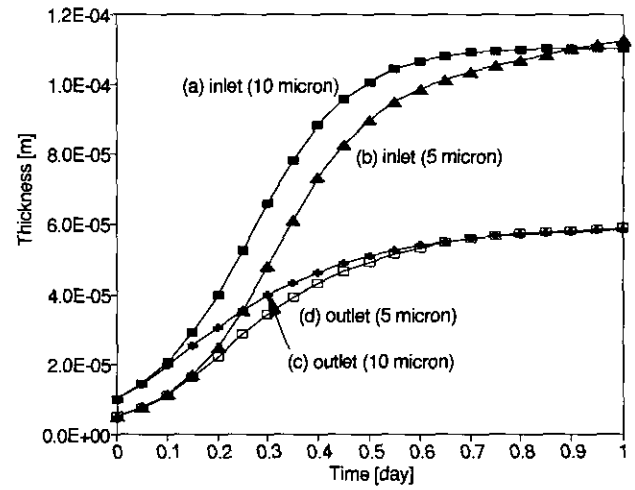

FIG. 10. Biofilm thickness L_F as a function of time (standard and run8).

converged within plotting accuracy, the standard run gives quantitatively reasonable predictions for engineering applications.

5.4. *Effect of Initial Thickness*

The effect of assuming a given initial biofilm thickness to start the simulations was also tested (run8). The result is shown in Fig. 10, whereby the initial thickness of the film was changed from 10μ to 5μ. The inlet and outlet thickness values as functions of time are shown for both the standard solution and the new one. As expected, both runs reach the same steady state values, but the time evolution of the new calculation lags behind that of the standard run.

5.5. *Multispecies Biofilm*

In order to test the algorithm proposed for a multispecies biofilm, a simple run was performed with two particulate components ($N_{\text{part}} = 2$). A second growth reaction was added ($N_{rxn} = 2$) to describe the growth of the new species (ps_1). The other species (ps_2) was assumed to have the same characteristics as pseudomonas in the standard run. The new reaction parameters read:

$$\nu_{2,\text{glu}} = -1.78, \quad \nu_{2,ps_1} = 1, \quad T_{2,\text{glu}} = \frac{Q_{\text{glu}}}{1.6 + Q_{\text{glu}}}, \qquad T_{2,ps_1} = 2 \times 10^{-4} Q_{ps_1} \quad \text{kg/m}^3, \tag{5.11}$$

It should be noted that ps_2 does not participate in this reaction, thus its reaction rate expression is of zero order with coefficient one, and its stoichiometry is zero (the same is true for ps_1 in the first reaction). Moreover, the rate of growth of ps_1 is twice that of ps_2; otherwise the two particulates are the same. The initial volume fractions (ε_{ps_1} and ε_{ps_2}) were both set to 0.1.

Computational results from this run are presented in Figs. 11 through 13. In Fig. 11 the inlet thickness values are shown as functions of time for the present two-species biofilm and compared with the standard run. Due to the faster growth of ps_1, the film grows significantly faster and reaches steady state before the standard case. However, the steady state thicknesses are practically the same. Figure 12 shows how the volume fractions of the two species at the interface change as functions of time at the inlet and the outlet. It is clear that the faster growing particulate (ps_1) very quickly outcompetes ps_2 and becomes the dominant species after $t = 0.1d$. It is also obvious that the lower concentration of glucose at the outlet results in a slower "takeover." Finally, Fig. 13 shows the axial profiles of the

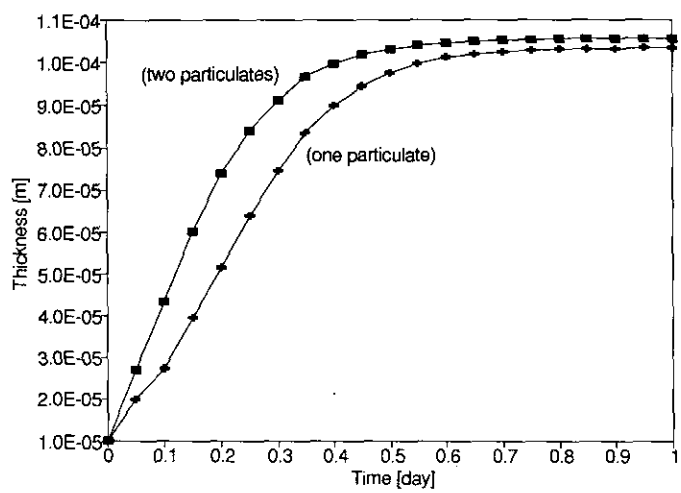

FIG. 11. Biofilm thickness L_F at the inlet for a single particulate (standard) and two particulates (run9).

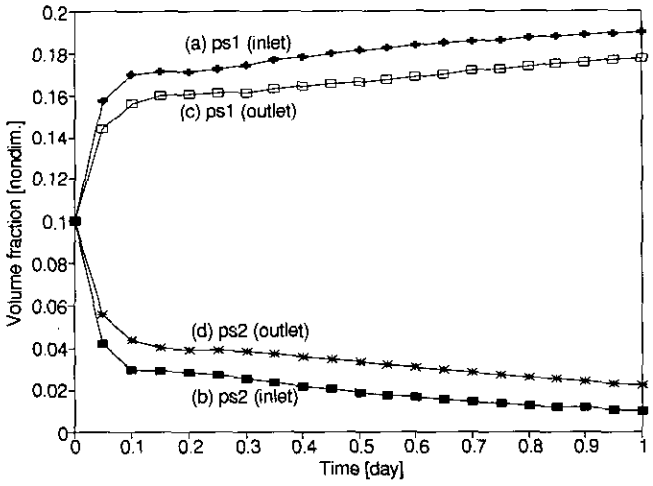

FIG. 12. Volume fractions of particulates versus time.

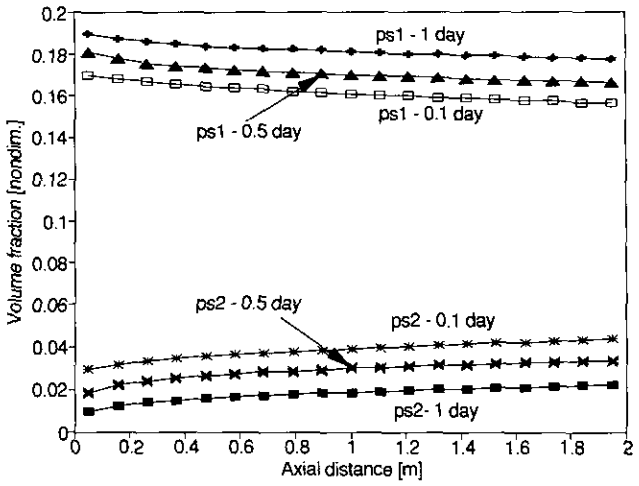

FIG. 13. Volume fractions of particulates versus axial distance.

volume fractions at $t = 0.1$, $t = 0.5$, and $t = 1$ days. Again, a gradient of volume fractions can be observed along the pipe, as a result of slower growth downstream.

5.6. *Operation Count*

The operation count for the present technique was estimated. In order to determine it, a sketch of the algorithm might be useful:

```
begin
    initialize system
    t = t_0
    while t < t_end
    begin
        calculate velocities
        calculate grid velocity
        move grid
        for all axial positions
        begin
            while not converge
            begin
                calculate Jacobians
                calculate fluxes
                build tridiagonal matrix
                solve system (Block-Thomas)
                update solution
                check convergence
            end
        end
        t = t + Δt
    end
end
```

The size of the problem is determined by the following parameters: number of components ($c = N_{part} + N_{sub}$), number of reactions ($r = N_{rxn}$) total number of radial grid points ($n = N_{rad} + N_{film}$), number of axial grid points ($m = N_{axial}$), number of iterations (N_{iter}), and number of timesteps to be performed ($N_{step} = (t_{end} - t_0)/\Delta t$). For simplicity a constant timestep is assumed. Since there are $(n-1)(m-1) = O(nm)$ volumes, calculating velocities takes $O(nm)$ time. The same time ($O(nm)$) is needed to calculate the grid velocities, since $O(m)$ time is needed to calculate the interface velocities, and $(m-1)(n-2) = O(nm)$ faces have to be moved. At every axial section there are $O(n)$ surfaces and for each surface four Jacobians (two viscous and two inviscid) of dimensions $c \times c$ are calculated, for a total of $4O(n)\, c^2 = O(nc^2)$. The same is true for fluxes, with the exception that instead of c^2 only c entries exist, thus it takes $O(nc)$ operations only. In order to calculate the reaction terms, $O(nr^2c)$ operations are needed (see Eq. (2.4)). To calculate the source term Jacobian, $O(nr^2c^3)$ operations are necessary. In order to solve the block-tridiagonal system $O(nc^3)$ operations are required [5]. This is a considerable improvement over the $O(n^3c^3)$ operations required if full Gauss elimination is used. Thus the overall operation count reads

$$T = O(N_{step}[O(nm) + (m-1)\, N_{iter}(O(nc^2) + O(nr^2c^3) + O(nc^3))]), \tag{5.12}$$

which reduces to

$$T = O(N_{step} N_{iter} mnr^2c^3). \tag{5.13}$$

The previous formula shows that the computational cost for larger problems will increase with the cubic power of the number of species, the square of the number of chemical reactions considered, and quadratically if the grid size in both directions is changed. Moreover, refining the grid can

lead to numerical stability problems, which might affect the required number of steps and lead to a more than quadratic dependence of the operation count from the grid size.

6. CONCLUSIONS

A finite-volume-based numerical technique has been introduced and described for the simulation of biofilm processes in closed conduits. The algorithm is able to resolve unsteady problems with multiple space and time scales and moving boundaries. The present methodology can be extended to three space dimensions and different reactor configurations, due to the geometric flexibility obtainable by means of finite volumes.

Future work requires including fluid dynamic and thermodynamic phenomena in the model, so that a coupled set of species continuity, global momentum, and energy equations can be discretized and solved. Moreover, work is in progress on the validation of the present approach by comparison with experimental data.

ACKNOWLEDGMENTS

This study is the result of the collaboration between the Center for Interfacial Microbial Process Engineering at Montana State University and the Engineering Research Center for Computational Field Simulation at Mississippi State University. Both centers are funded in part by the National Science Foundation. The first and third authors wish to acknowledge Cooperative Agreement ECD-8907039 between the National Science Foundation and Montana State University.

REFERENCES

1. W. G. Characklis *et al.*, IAWPRC Scientific and Technical Report, 1989 (unpublished).
2. W. G. Characklis and K. C. Marshall (Eds.), *Biofilms* (Wiley, New York, 1990).
3. *In Process*, newsletter, Center for Interfacial Microbial Process Engineering, Montana State University, Spring 1992.
4. O. Wanner and W. Gujer, *Biotechnol. Bioeng.* **28**, 314 (1986).
5. C. A. J. Fletcher, *Computational Techniques for Fluid Dynamics* (Springer-Verlag, New York, 1988).
6. B. Van Leer, J. L. Thomas, P. L. Roe, and R. W. Newsome, "A Comparison of Numerical Flux Formulas for the Euler and Navier–Stokes Equations," AIAA Paper No. 87-1104-CP, 1987.
7. R. H. Notter and C. A. Sleicher, *Chem. Eng. Sci.* **26**, 161 (1971).
8. J. M. Janus, Ph.D. dissertation, Mississippi State University, 1989 (unpublished).
9. P. D. Thomas and C. K. Lombard, *AIAA J.* **17**, 1030 (1979).
10. B. Grossman and R. W. Walters, *AIAA J.* **27**, 524 (1989).
11. P. L. Roe, *Annu. Rev. Fluid Mech.* **18**, 337 (1986).
12. R. W. Walters, P. Cinnella, D. C. Slack, and D. Halt, *AIAA J.* **30**, 1304 (1992).
13. L. B. Simpson and D. L. Whitfield, *AIAA J.* **30**, 914 (1992).